VIII. APPENDIX A
Raw Materials Used and Method of Pellet Manufacture

8.1 Introduction

The processes used to manufacture manganese-based pellets used in this study essentially comprise mixing combinations of manganese-containing compounds and an alumina-based matrix material with organic or inorganic binders. The mixed powder is then fed to a pelletizer, along with a fine spray of water to form spherical pellets. These pellets are dried to impart green strength for further handling. The dried pellets are then indurated at high temperature to obtain the desired combination of physical properties such as crush strength and porosity.

The raw materials used to form the pellets comprise a source of manganese as either a carbonate or an oxide ore and an alumina-based matrix to provide the strength needed to maintain porosity and provide the mechanical structure in the pellets. In the compositions employing manganese carbonate, preliminary work indicated that it is preferred to also include an inorganic binder to provide further cementing actions to increase strength in the pellets as well as to facilitate formation into spherical pellets. In compositions employing manganese oxides, the raw materials can include an organic binder to provide additional porosity to the pellets as the organic binder volatilizes during induration as well as to provide a mechanism for formation of the raw materials into pellets. Organic binders can also be included in formulations using manganese carbonates, but are typically not needed because of the porosity-enhancing effects of $MnCO_3$ dissociation.

The leading formulation (FORM4-A), a combination of technical grade manganese carbonate, alundum, and bentonite as an inorganic binder, provides excellent sulfidation and regeneration characteristics. No further modifiers or surface area or porosity promoters are needed since the carbonate, upon dissociation and volatilization of the contained carbon dioxide during induration of the pellets, produces the required porosity.

The spherical shape of the pellets and the high crush strength imparted to them by the presence of the inorganic binder result in desirable handling and packing characteristics. The inorganic binder also preferably provides a strong, permanent bridging action between manganese oxide and matrix materials. It should be noted that the amount of inorganic binder is preferably limited, not only to reduce the cost of the finished pellets, but also to provide a greater amount of chemically active sorbent to maximize both sorption capacity and reaction rates.

Another problem faced by many of the pellet-based sorbent systems is that the pellets are typically formed through extrusion processes which provide essentially cylindrical-shaped pellets. Although cylindrical pellets are expedient from a manufacturing standpoint, they do not provide optimum packing efficiency. Furthermore, the cylindrical pellets have edges at either end which are the center of stress and the site of degradation of the pellets, resulting in the loss of sorbent capacity.

The preferred inorganic binder comprises bentonite, although other

inorganic binders, such as kaolin or Portland cement could be substituted for bentonite. The presence of the organic binder dextrin also enhances the porosity as this material burns away during the induration process. Other organic binders which could be used in the process include starches, methyl cellulose, and molasses.

In the formulations comprising manganese carbonate, precalcination mass of the $MnCO_3$ was chosen to produce 75% by weight MnO in the finished pellets because calcination of manganese carbonate effectively reduces its mass upon loss of carbon dioxide.

The preferred particle sizes of both the manganese compounds and matrix compounds is less than about 100 μm, and more preferably less than about 50 μm to facilitate pellet formation.

8.2 Pellet Preparation Procedure

Feed is prepared by adding a binder to the dry mix of manganese-containing compound and alumina-based matrix and mulling the mixture while slowly adding water to produce a cohesive, but not sticky, consistency. The amount of water needed is typically in the range of about 5 to 10% by weight.

The mix is then rubbed through a 10-mesh sieve to form fines. Pelletization is accomplished using a balling tire at a 40 to 60° inclination to the horizontal and a rotational speed of 30 to 50 rpm. Initially, the tire interior is moistened and then wiped clean. About 7% by weight of the prepared feed in the form of fines is slowly sprinkled into the rotating tire. When seeds begin to form (as evinced by micro-pellets), moisture is added in discrete increments (of about 0.1% by weight of the original solids) via a finely atomized hand-held sprayer (spray droplets 5 to 15 μm in diameter) along with additional fines to allow the seeds to grow. After growth, the seeds are removed and screened to pass a 6-mesh screen, and the fines are returned to the tire.

This procedure is continued until approximately one-third of the original feed (which is set aside) is converted to agglomerates which would ideally range in size from 2 to 5 mm in diameter. At this point, the feed is divided into three portions. In the subsequent pellet making operation, a portion of the seeds is returned to the tire and sprayed with the above fine spray of water until the glistening point is noted. This glistening point is a visual observation of a shiny reflective surface appearance on pellets which originally appeared as "flat", i.e. non-glossy. Fines are then added in small increments to cause the seeds to grow.

The rate of addition of fines is controlled so as to avoid sticking and also to promote the free-rolling of the pellets. Too slow a rate of addition causes the seeds to stick together; whereas, too rapid an addition causes the formation of unnecessary new seeds in competition with the desired growth of the original seeds. Immediately after this procedure of addition of the fines, water is sprayed once again to bring the pellets to the glistening point. This procedure of spraying pellets to the glistening point and the subsequent addition of fines is

repeated until the pellets grow to the desired final size. At this point, the pellets are removed from the pelletizer and screened; the 7- to 10-mm fraction is stored in desiccators pending evaluation of their strength and appearance, and the undersize pellets are returned to the tire for further growth.

The required moisture content for the feed depends on its average density. Balling is optimal at about 30-35% moisture on a volume basis, i.e., the approximate void fraction in dried pellets. For 33% moisture on a volume basis, it can be shown that the required amount of water to be added is given by the following equation:

$$Wt.\%(H_2O) = \frac{100}{\left[1 + \frac{67}{33}\,\rho_{av}\right]} \qquad (8.1)$$

where ρ_{av} is the average density of the feed.

The green pellets are then dried to a constant weight at 110 °C and then indurated. Induration was conducted for a 12 hour cycle in air and involved heating from 25 °C to about 300 °C over one hour; heating from about 300 °C to about 400 °C over a period of about five hours and then holding the Moanda ore based pellets at 1200 °C for one to two hours while the manganese based pellets were heated to about 1250 °C and held there for one to two hours.

The pellets produced using the above procedures had the desired strength of greater than 22 N/mm of pellet diameter (5 lbs/mm).

8.3 Discussion

Some of the research discussed in Chapter 2 above has indicated that manganese based pellets may provide a useful sorbent for coal gas desulfurization at high temperature. None of the research, however, has provided a formulation of pellets and a process of manufacturing them which is economically feasible and provides pellets which have the characteristics necessary for successful commercial application. The durability provided both by the materials used to manufacture the pellets as well as their spherical shape allows the pellets to maintain their desired physical and chemical characteristics in long-term cyclic sulfidation and regeneration in a high-temperature desulfurization operation. The desired physical characteristics of pellets include high crush strength, resistance to attritioning or physical disintegration, and high porosity. The desired chemical characteristics are: a high sulfur sorption capacity (gS/100 g pellets) during the sulfidation step; and a high reaction rate and extent for both sulfidation and regeneration. The sorbent pellets are also produced by a relatively inexpensive process which uses commercially available reagents. The pelletizing operation requires the following commercially available equipment: mix-muller, pelletizer, drying oven, and induration furnace.

The spherical shape of the pellets manufactured by the process described above and the high crush strength imparted to them by the presence of the

inorganic binder, bentonite, result in desirable handling and packing characteristics. The increased packing density of spherical pellets as compared to typical cylindrical pellets allows more sorbent material to be contained within a reactor. That results in increased capacity as well as reaction rate. The spherical shape also eliminates the edges which are the site of degradation due to stresses during use as well as handling of typical cylindrical pellets.

8.4 Raw Materials Used and Their Assays

1) Regular Manganese Carbonate: Obtained from Chemetals, Inc. in Baltimore, MD. This product contains approximately 93-95% $MnCO_3$; no typical analysis is available at the present time.

2) Alundum Fepa F, Size 600, Code 7102: Obtained from Industrial Ceramics Corporation (Norton Materials) in Worcester, MA.

Table 8.1 Typical Chemical Analysis of Alundum

Species	Al_2O_3	TiO_2	SiO_2	Fe_2O_3	CaO	MgO	S	K_2O
Wt.%	96.60	2.60	0.60	0.20	0.10	0.40	0.02	0.02

3) Manganous Oxide (MnO) Ore, Industrial Grades: Received from Chemetals, Inc. This product contains approximately 60% manganese.

Table 8.2 Chemical Analysis of Manganous Oxide Ore Used in Preliminary Work.

Ingredient	Approximate %
Manganese Oxide	55 - 83
Manganese Tetroxide	75 - 85
Iron as Iron Oxide	4 (max.)
Silica as Silicon Oxide	5 (max.)
Aluminum Dioxide	8 (max.)
Barium as Barium Compounds	4 (max.)

4) Bentonite, an inorganic binder, was obtained from the Aldrich Chemical Company, Inc. in Milwaukee, WI.

5) Dextrin (type IV), an organic binder, was obtained from the Sigma Chemical Company in St. Louis, MO.

6) "Moanda" Ore (African Manganese Dioxide Ore) and "GE" Ore (Australian Manganese Dioxide Ore): Obtained from The Prince Manufacturing Company in Quincy, Il.

Table 8.3 Typical Chemical Analysis of Two Foreign Manganese Ores

Comilog (African) Ore

Species	Wt.%
Mn	51.2
MnO_2	77.0
MnO	3.36
Al_2O_3	6.01
Fe	2.81
SiO_2	2.56
K_2O	0.71
BaO	0.22
TiO_2	0.22
P	0.109
Co	0.099
CaO	0.08
Zn	0.064
MgO	0.06
Ni	0.058
Cu	0.05
CO_2	0.04
Na_2O	0.04
S	0.019
V	0.012
As	0.007
Cr	0.006
Mo	0.006
Pb	0.004
H_2O (bound)	5.16

Australian Ore

Species	Wt.%
Mn	52.8
MnO_2	83.6
Al_2O_3	3.4
Fe	2.2
SiO_2	2.8
BaO	1.86
K_2O	1.25
Na_2O	0.21
MgO	0.2
SrO	0.16
TiO_2	0.13
P	0.06
CaO	0.05
V	0.03
Zn	0.019
Co	0.015
Ni	0.013
Cu	0.008
Pb	0.005
As	0.005
F	0.006
Cl	0.005
S	0.005
Cr	0.003
Mo	0.004
Sb	0.001
B	0.001
Li	0.001
W	0.001
Cd	0.0005
H_2O (bound)	3.4

IX. APPENDIX B
Derivation of Relevant Kinetic Expressions

9.1 Definition of symbols used and their units

S_{ex}: exterior surface of pellet (fresh, fully-loaded, or recycled), cm^2
S_c: exterior surface of unreacted pellet core, cm^2
r_i'': reaction rate per unit surface area, mol/cm^2-s
N: number of moles of reactive component (MnO or MnS), mol
t: reaction time, s
R_p: radius of reduced or regenerated pellet, cm
k_g: mass transfer coefficient between gas phase and sorbent pellet, cm/s
k_s: first-order rate constant for the surface reaction, cm/s
C_i: concentration of gaseous component i, mol/cm^3
Superscript s: value of parameter at surface
Superscript o: initial value of parameter
Superscript e: equilibrium value of parameter at reaction site
ρ_i: molar density of reactive component i in pellet, mol/cm^3
V: volume of pellet, cm^3
r: arbitrary position within radius of pellet, cm
r_c: radius of unreacted pellet core, cm
τ_{gf}: time for complete reaction when diffusion through gas film is rate-limiting, s
τ_{pl}: time for complete reaction when diffusion through product layer is rate-limiting, s
τ_{sr}: time for complete reaction when surface reaction is rate-limiting, s
F_i: fractional conversion of reactive component i as a function of time, dimensionless
J_i: molar flux of gaseous component i, mol/cm^2-s
D_e: effective diffusivity, cm^2/s
y_i: mole fraction of component i in the gas phase, dimensionless
R: universal gas constant, cm^3-atm/mol-°K
T: absolute reaction temperature, °K
P: total pressure, atm
J: total molar flux, mol/cm^2-s
P_i: partial pressure of gaseous component i, atm

9.2 Introduction

The sulfidation reaction is represented by equation (9.1):

$$MnO_{(s)} + H_2S_{(g)} = MnS_{(s)} + H_2O_{(g)} \qquad (9.1)$$

while the overall regeneration reaction is represented by equation (9.2):

$$MnS_{(s)} + \frac{5}{3} O_{2(g)} = \frac{1}{3} Mn_3O_{4(s)} + SO_{2(g)} \qquad (9.2)$$

Both reactions are heterogeneous in which a gas contacts a solid, reacts with it, and transforms it into products. In both cases the pellets contain sufficient

amounts of non-reactive (inert) impurities (alundum matrix and inorganic binder in some instances) which remain as a non-flaking materials. Both reactions also form firm product material, i.e., sulfide or oxide of somewhat similar specific volumes. Accordingly, the sorbent pellets may be assumed to remain unchanged in size during sulfidation and regeneration, although they undergo structural changes. Such an assumption is made in the modeling of metallurgical processes such as the roasting of sulfide ores and the subsequent reduction of the resulting oxides to metals. In addition, the sulfidation and regeneration reactions are controlled to a large extent by diffusion and may thus be considered irreversible. An additional assumption may be made about the reaction being elementary (i.e., first-order with respect to H_2S) and the concentration gradients being linear to simplify the mathematical treatment of the problem and obtain an analytical solution.

For the non-catalytic reactions of particles with surrounding gas two simple idealized models have been conceptualized: the *progressive-conversion model* and the *shrinking-core model*. In the former model the reactant gas enters and reacts throughout the particle at all times, i.e., the solid reactant is converted continuously and progressively throughout the particle. In the latter model the reaction proceeds at a narrow front which moves into the solid particle and the reactant is completely converted as the front progresses.

Evidence from a wide variety of situations indicates that the shrinking-core model approximates the behavior of real particles more closely in most cases than does the progressive-conversion model. Therefore, in the following analysis, rate equations (time-conversion) describing the progress of the sulfidation reaction with time have been derived (with reference to Figure 4.10 in Chapter 4). Those equations describing the progress of the regeneration reaction with time were also derived using the same approach, but only the case where gaseous diffusion through the product layer is rate-limiting is considered.

9.3 Application of the Shrinking-Core Model for Spherical Pellets During Sulfidation

Five steps are conceptualized to occur in series during the sulfidation reaction:

Step 1: Diffusion of gaseous reactant H_2S through the gas film surrounding the pellet to the exterior surface of the pellet;

Step 2: Penetration and diffusion of H_2S through the newly-formed product layer, MnS, to the surface of the unreacted core;

Step 3: Reaction of H_2S with the reactive component, MnO, at the reaction front to exchange sulfur with oxygen and release H_2O;

Step 4: Diffusion of the gaseous product, H_2O, through the product layer, MnS, to the exterior surface of the pellet; and

Step 5: Diffusion of H_2O through the gas film to the bulk of the reducing fuel gas.

It must be noted that diffusion steps 2 and 4 could be considered as one

step as a countercurrent diffusion in a binary gas mixture. The resistances of the different steps usually vary greatly from one another and the step with the highest resistance is taken as the rate-controlling step.

9.3.1 Diffusion through gas film controls:

In this case the concentration profile for gaseous reactant H_2S is as depicted in Figure 4.10(a) which shows that no reactant is present at the exterior surface of the pellet (S_{ex}) or at the surface of the unreacted core (S_c). When diffusion through the gas film is rate-limiting, diffusion through the product layer and the surface reaction are relatively fast that the exit reactant gaseous component is immediately consumed as soon as it gets to the surface.

It is convenient to derive the relevant kinetic expressions based on the unchanging exterior surface of the pellet (S_{ex}). The following procedure is initiated by the selection of one reaction component; the reaction rate is then defined in a meaningful way in terms of this component. Although initially the manganese exists as Mn_3O_4 in the indurated fresh pellet, the reactive constituent of the pellet, MnO, serves the purpose of defining the reaction rate best. It must be pointed out that MnO is the thermodynamically stable form of manganese in the pellet upon its exposure to the reducing fuel gas, as established in Chapters 3 and 4. Based on unit exterior surface of the pellet in this gas-solid system the reaction rate is given by:

$$r''_{MnO} = -\frac{1}{S_{ex}}\frac{dN_{MnO}}{dt} = \frac{\textit{Moles of MnO reacted}}{(\textit{exterior surface of pellet})\ (\textit{time})} \tag{9.3}$$

$$-\frac{1}{S_{ex}}\frac{dN_{MnO}}{dt} = -\frac{1}{4\pi R_p^2}\frac{dN_{MnO}}{dt} = -\frac{1}{4\pi R_p^2}\frac{dN_{H_2S}}{dt} = k_g(C^{\circ}_{H_2S} - C^{e}_{H_2S}) \tag{9.4}$$

If we let ρ_{MnO} be the molar density of MnO in the pellet and V the volume of the *reduced* pellet, then the number of moles of MnO present in the reduced pellet is given by:

$$N_{MnO} = \rho_{MnO} V \tag{9.5}$$

The change in the number of moles of reactive component MnO which causes the volume or the radius of unreacted core to decrease is then given by:

$$-dN_{MnO} = -dN_{H_2S} = -\rho_{MnO}\, dV = -\rho_{MnO}\, d(\frac{4}{3}\pi r_c^3) = -4\pi\rho_{MnO}\, r_c^2 dr_c \tag{9.6}$$

The rate of reaction can then be written in terms of the shrinking radius of unreacted core as follows:

$$-\frac{1}{S_{ex}}\frac{dN_{MnO}}{dt} = -\frac{\rho_{MnO}\, r_c^{\,2}}{R_p^{\,2}}\frac{dr_c}{dt} = k_g(C^{\,o}_{H_2S} - C^{\,e}_{H_2S}) \qquad (9.7)$$

We then separate the variables and integrate to get an expression describing the shrinkage of the unreacted core with time:

$$-\frac{\rho_{MnO}}{R_p^{\,2}}\int_R^{r_c} r_c^{\,2}\,dr_c = k_g(C^{\,o}_{H_2S} - C^{\,e}_{H_2S})\int_0^t dt \qquad (9.8)$$

from which we can deduce time t as follows:

$$t = \frac{\rho_{MnO}\, R_p}{3k_g(C^{\,o}_{H_2S} - C^{\,o}_{H_2S})}\left[1 - \left(\frac{r_c}{R}\right)^3\right] \qquad (9.9)$$

The time τ_{gf} for complete reaction of the pellet is obtained by setting $r_c=0$:

$$\tau_{gf} = \frac{\rho_{MnO}\, R_p}{3k_g(C^{\,o}_{H_2S} - C^{\,e}_{H_2S})} \qquad (9.10)$$

Equation (9.9) may then be written in terms of τ_{gf}, as follows:

$$\frac{t}{\tau_{gf}} = 1 - \left(\frac{r_c}{R_p}\right)^3 \qquad (9.11)$$

The fractional conversion of MnO is defined as:

$$F_{MnO} = \frac{N^{\,o}_{MnO} - N_{MnO}}{N^{\,o}_{MnO}} = 1 - \frac{\frac{4}{3}\pi r_c^{\,3}\rho_{MnO}}{\frac{4}{3}\pi R_p^{\,3}\rho_{MnO}} = 1 - \left(\frac{r_c}{R_p}\right)^3 \qquad (9.12)$$

It follows that:

$$\frac{t}{\tau_{gf}} = 1 - \left(\frac{r_c}{R_p}\right)^3 = F_{MnO} \qquad (9.13)$$

An important relationship between time, pellet size (radius), and fractional conversion for the case where diffusion of H_2S through the gas film controls is given by:

$$F_{MnO} = \frac{3k_g(C^o_{H_2S} - C^e_{H_2S})}{\rho_{MnO} R_p} t + C_1 \qquad (9.14)$$

where C_1 is a constant of integration.
Given that:

$$C_i = \frac{P_i}{RT} \qquad (9.15)$$

equation (9.14) becomes:

$$F_{MnO} = \frac{3k_g(P^o_{H_2S} - P^e_{H_2S})}{RT\rho_{MnO} R_p} t + C_1 \qquad (9.16)$$

9.3.2 Diffusion through product layer controls:

During the consideration of the concentration gradient of gaseous reactant H_2S, it is reasonable to assume that the unreacted core is stationary. With this steady state assumption the rate of reaction of H_2S at any instant is given by its rate of diffusion to the reaction site, as given by the following equation:

$$-\frac{dN_{H_2S}}{dt} = 4\pi r^2 J_{H_2S} = 4\pi R_p^2 J^s_{H_2S} = 4\pi r_c^2 J^c_{H_2S} \qquad (9.17)$$

If we let the flux of H_2S through the product layer (MnS) be expressed by Fick's law for equimolar counterdiffusion, then we obtain:

$$J_{H_2S} = D_e \frac{dC_{H_2S}}{dr} \qquad (9.18)$$

where D_e is the effective diffusion coefficient (diffusivity) of gaseous reactant H_2S in the product layer. Combining equations (17) and (18), we get:

$$-\frac{dN_{H_2S}}{dt} = 4\pi r^2 D_e \frac{dC_{H_2S}}{dr} \qquad (9.19)$$

Integrating across the product layer, we get:
This reduces to the following differential equation which describes the conditions

$$-\frac{dN_{H_2S}}{dt}\int_{R_p}^{r_c}\frac{dr}{r^2} = 4\pi D_e \int_{C^o_{H_2S}-C^e_{H_2S}}^{C^e_{H_2S}-C^e_{H_2S}} dC_{H_2S} \qquad (9.20)$$

of a reacting particle at any time t:

$$-\frac{dN_{H_2S}}{dt}\left(\frac{1}{r_c} - \frac{1}{R_p}\right) = 4\pi D_e(C^o_{H_2S} - C^e_{H_2S}) \qquad (9.21)$$

This equation contains three variables: t, N_{H2S}, and r_c, one of which must be eliminated or expressed in terms of the other variables before integration can be performed to obtain an analytical solution. N_{H2S} may be eliminated by writing it in terms of r_c, as follows:

$$-\rho_{MnO}\int_{r_c=R_p}^{r_c}\left(\frac{1}{r_c} - \frac{1}{R_p}\right)r_c^2 dr_c = D_e(C^o_{H_2S} - C^e_{H_2S})\int_0^t dt \qquad (9.22)$$

or

$$t = \frac{\rho_{MnO}\,R_p^2}{6D_e(C^o_{H_2S} - C^e_{H_2S})}\left[1 - 3\left(\frac{r_c}{R}\right)^2 + 2\left(\frac{r_c}{R}\right)^3\right] \qquad (9.23)$$

For complete conversion of the pellet, $r_c=0$, and the time required is:

$$\tau_{pl} = \frac{\rho_{MnO}\,R_p^2}{6D_e(C^o_{H_2S} - C^e_{H_2S})} \qquad (9.24)$$

Equation (23) can then be expressed in terms of τ_{pl}, as follows:

$$\frac{t}{\tau_{pl}} = 1 - 3\left(\frac{r_c}{R_p}\right)^2 + 2\left(\frac{r_c}{R_p}\right)^3 \qquad (9.25)$$

or in terms of fractional conversion, we get:

$$\frac{t}{\tau_{pl}} = 1 - 3(1 - F_{MnO})^{2/3} + 2(1 - F_{MnO}) \qquad (9.26)$$

$$3 - 2F_{MnO} - 3(1 - F_{MnO})^{2/3} = \frac{6D_e(C^o_{H_2S} - C^e_{H_2S})}{\rho_{MnO} R_p^2} t + C_2 \qquad (9.27)$$

where C_2 is a constant of integration. Combining equation (9.27) and equation (9.15), we get:

$$3 - 2F_{MnO} - 3(1 - F_{MnO})^{2/3} = \frac{6D_e(P^o_{H_2S} - P^e_{H_2S})}{RT\rho_{MnO} R^2_p} t + C_2 \qquad (9.28)$$

9.3.3. Chemical (surface) reaction controls:

In this case the progress of reaction is independent of the existence of the gas film or the product layer. The reaction rate is thus proportional only to the available surface of the unreacted core. Therefore, the rate of reaction is given by:

$$-\frac{1}{4\pi r_c^2}\frac{dN_{MnO}}{dt} = -\frac{1}{4\pi r_c^2}\frac{dN_{H_2S}}{dt} = k_s(C^o_{H_2S} - C^e_{H_2S}) \qquad (9.29)$$

where k_s is the first-order rate constant for the surface reaction . N_{MnO} is then expressed in terms of the shrinking radius r_c, as follows:

$$-\frac{1}{4\pi r_c^2}\rho_{MnO}4\pi r_c^2\frac{dr_c}{dt} = -\rho_{MnO}\frac{dr_c}{dt} = k_s(C^o_{H_2S} - C^e_{H_2S}) \qquad (9.30)$$

Separating variables and integrating, we get:

$$-\rho_{MnO}\int_{R_p}^{r_c} dr_c = k_s(C^o_{H_2S} - C^e_{H_2S})\int_0^t dt \qquad (9.31)$$

The time τ_{sr} for complete conversion is determined by setting $r_c=0$:

$$t = \frac{\rho_{MnO}}{k_s(C^{\circ}_{H_2S} - C^{e}_{H_2S})}(R_p - r_c) \tag{9.32}$$

$$\tau_{sr} = \frac{\rho_{MnO}\, R_p}{k_s(C^{\circ}_{H_2S} - C^{e}_{H_2S})} \tag{9.33}$$

$$\frac{t}{\tau_{sr}} = 1 - \frac{r_c}{R_p} = 1 - (1 - F_{MnO})^{1/3} \tag{9.34}$$

Again, a more useful equation is in the form:

$$1 - (1 - F_{MnO})^{1/3} = \frac{k_s(C^{\circ}_{H_2S} - C^{e}_{H_2S})}{\rho_{MnO}\, R_p}\, t + C_3 \tag{9.35}$$

where C_3 is a constant of integration.

$$1 - (1 - F_{MnO})^{1/3} = \frac{k_s(P^{\circ}_{H_2S} - P^{e}_{H_2S})}{RT\rho_{MnO}\, R_p}\, t + C_3 \tag{9.36}$$

9.4 Application of the Shrinking-Core Model for Spherical Pellets During Regeneration

The regeneration reaction is irreversible; in addition, its highly exothermic nature makes it even more likely to be controlled by countercurrent diffusion of oxygen and sulfur through the porous Mn_3O_4 product layer. For these reasons, only the derivation of the equation when diffusion through product layer is rate-limiting is deemed worthwhile. As was established above, the overall regeneration reaction is represented by equation 9.2.

The molar flux of O_2 through the newly-formed Mn_3O_4 layer is expressed by Fick's law, as follows:

$$J_{O_2} = -D_e \frac{dC_{O_2}}{dr} + y_{O_2} J \tag{9.37}$$

The first term on the right-hand side of the above equation is termed molecular diffusion flux and is produced by a concentration gradient; the second term represents the flux resulting from the bulk motion of the regeneration gas. J is the total flux, and is given by:

$$J = J_{O_2} + J_{SO_2} \tag{9.38}$$

From the stoichiometry of the overall regeneration reaction, the following relation applies:

$$J_{SO_2} = -\frac{3}{5} J_{O_2} \tag{9.39}$$

Substituting for J in terms of J_{O2} in equation (9.37) and rearranging, we get:

$$(1 - \frac{2}{5} y_{O_2}) J_{O_2} = -D_e \frac{dC_{O_2}}{dr} \tag{9.40}$$

With the assumption of steady state (i.e, stationary unreacted core), the rate of reaction of O_2 as a function of time is given by its rate of diffusion to the reaction site, as expressed by the following equation (similar to equation (9.17)):

$$\frac{-dN_{O_2}}{dt} = 4\pi r^2 J_{O_2} = 4\pi r^2 \left[\frac{-D_e}{1 - \frac{2}{5} y_{O_2}}\right] \frac{dC_{O_2}}{dr} \tag{9.41}$$

Integrating across the product layer, we get:

$$\frac{dN_{O_2}}{dt} \left(\frac{1}{r_c} - \frac{1}{R}\right) = -4\pi D_e \int_{C^*_{O_2}}^{C^*_{O_2}} \left[\frac{dC_{O_2}}{1 - \frac{2}{5} y_{O_2}}\right] \tag{9.42}$$

Recognizing that:

$$C_{O_2} = \frac{P_{O_2}}{RT} \tag{9.43}$$

and that:

$$y_{O_2} = \frac{P_{O_2}}{P} \tag{9.44}$$

we obtain the following differential equation which describes the conditions of the pellet during the course of the regeneration reaction:
Following a similar procedure as the one above for the case of the sulfidation

$$\frac{dN_{O_2}}{dt}\left(\frac{1}{r_c} - \frac{1}{R}\right) = \frac{10\pi D_e P}{RT} \ln\left[\frac{5P - 2P^e_{O_2}}{5P - 2P^o_{O_2}}\right] \qquad (9.45)$$

reaction, it can be shown that N_{O2} may be eliminated by writing it in terms of r_c, as follows:

$$dN_{O_2} = \frac{20}{3}\rho_{MnS}\pi r_c^2 dr_c \qquad (9.46)$$

Separating variables and integrating, we get the following equation in terms of the fractional conversion of manganese sulfide in the sulfided (loaded) pellet (F_{MnS}):

$$3-2F_{MnS}-3(1 - F_{MnS})^{2/3} = \frac{9D_e P}{RT\rho_{MnS} R_p^2} \ln\left[\frac{5P - 2P^e_{O_2}}{5P - 2P^o_{O_2}}\right] t+C_4 \qquad (9.47)$$

where C_4 is a constant of integration.

The time-conversion equations derived above are summarized in the following table.

Table 9.1 Time-Conversion Performance Equations for Sulfidation and Regeneration Reactions Using the Shrinking Unreacted-Core Model.

Rate-Limiting	Sulfidation Reaction	Regeneration Reaction
Gas Film	$F_{MnO} = \frac{3k_g(P^{\circ}_{H_2S} - P^{e}_{H_2S})}{RT\rho_{MnO}\, R_p}\, t + C_1$	
Product Layer	$3 - 2F_{MnO} - 3(1 - F_{MnO})^{2/3} = \frac{6D_e(P^{\circ}_{H_2S} - P^{e}_{H_2S})}{RT\rho_{MnO}\, R_p^2}\, t + C_2$	$3-2F_{MnS}-3(1 - F_{MnS})^{2/3} = \frac{9D_eP}{RT\rho_{MnS}\, R_p^2} \ln\left[\frac{5P - 2P^{e}_{O_2}}{5P - 2P^{\circ}_{O_2}}\right] t+C_4$
Surface Reaction	$1 - (1 - F_{MnO})^{1/3} = \frac{k_s(P^{\circ}_{H_2S} - P^{e}_{H_2S})}{RT\rho_{MnO}\, R_p}\, t + C_3$	

X. APPENDIX C
Petrographic Study of Mn Oxide and Sulfide Pellets

Acknowledgements. The author thanks Dr. Rolland Blake of the Twin Cities Research Center of the U.S. Bureau of Mines for carrying out this study. This appendix is based entirely on Dr. Blake's report.

10.1 Introduction

Manganese-based pellets, in the fresh (oxide) and loaded (sulfide) conditions, are characterized by using light optical microscopy (LOM), X-ray diffraction (XRD), and electron microprobe analyses (EMP). The purpose of this study is to determine macro- and micro-structure and macro- and micro-texture, the crystalline phases and degree of non-crystallinity, and the microchemistry of the pellets. The ultimate goal is to gain further understanding of the behavior of the pellets and improve their performance in the desulfurization of coal-derived fuel gases at high temperature.

The oxidation heating or induration would drive off any remaining moisture and CO_2 (in the case of $MnCO_3$ pellets) and result in an apparent chemistry of Mn_3O_4 crystals in an Al_2O_3-rich matrix for the oxide pellets.

10.2 Pellet Macrophotography and Macrocharacteristics

The size, shape, and color of FORM4-A pellet samples in the fresh and loaded condition are depicted in Figure 10.1. Fresh pellet: dull black color, spherical, and 3-4 mm in diameter. The sulfide pellet has a greenish-gray color. The same properties for FORM1-A pellets are depicted in Figure 10.2. Fresh pellet: dull brownish black, slightly oval 4-6 mm in diameter. The sulfide pellet has dull gray black color.

Pellet surface texture and fractures are shown in Figures 10.3 and 10.4. Most pellets showed one or more macrocracks, but one of the FORM4-A loaded pellets exhibited only one minor crack with a small hole; the other showed no surface cracks. The very fine texture of FORM4-A pellets is indicative of very fine grind of starting pelletizing materials.

10.3 Pellet Preparation

The pellets were briquetted in a monomer and hardened at room temperature with a catalyst. The polymerized briquette surface was ground on a resin- or metal-bonded lap until the pellet center was exposed. It was then polished by hand using 30, 16, 5, and finally 3 micron diamonds in a paste on a cloth lap. Pellet cavities exposed on the sectioned surface were purposely not filled with resin in order to reduce the number of grinding and polishing steps so as to preserve the actual texture and structure. Several pellet surfaces showed depressed areas where initial polishing marks were visible, but further polishing pressure had caused the surface to collapse as a result of the weak, highly porous pellet structure.

10.4 Pellet Photomicrography and Microcharacteristics

The polished pellet sections are shown in photomicrographs as Figures 10.5 through 10.8 (part a). Pellet structure is readily seen at this low magnification (34x) as highly porous and permeable (i.e., interconnected pores), with concentric ring agglomeration structure. Figure 10.5 (a) shows small to large black cavities and a collapse area within the large cavity of FORM4-A at the 9 to 10 o'clock

position. The white phase (highly reflective) appears to be scattered and somewhat interconnected within the medium gray matrix. The texture (grain to grain relationship) looks fairly uniform from edge to center. Figure 10.6 (a) of the partially reacted FORM4-A pellet shows a highly variable pellet texture. The center appears to be mostly a gray phase, the outer rim a mixture of light phase within a gray phase, and the mid-rim area has both many cavities and clumps of lighter phase within a matrix of gray phase. Figure 10.7 (a) shows FORM1-A pellet with a series of partly interconnected concentric cavities from the outer rim to near the center, plus an irregular central cavity. The white phase appears to be rather uniformly distributed as isolated irregular blebs. Figure 10.8 (a) shows that the partially sulfided FORM1-A pellet has a contiguous concentric cavity, central separated cavities, and slightly patchy distribution of white and gray phases. FORM4-A pellets appear to have a more even distribution and uniformity of size of white phase than FORM1-A pellets.

At moderate magnification (118x) Figures 10.5 through 10.8 (part b) show pellet fine texture. Figure 10.5 (b) shows that FORM4-A fresh pellet, at a location about 1/3 of the distance from edge to center, has the white phase highly interconnected at the smallest scale, but mostly separated by gray matrix at a larger scale. Some of the white phase is at cavity walls and much is within the gray phase. Figure 10.6 (b) shows that FORM4-A partially-reacted pellet (at about mid-rim location) has a more diffuse white phase in gray phase than in the fresh pellet. Figure 10.7 (b) for FORM1-A fresh pellet shows a somewhat smaller white phase with less interconnection than in the FORM4-A fresh pellet. FORM4-A partially-reacted pellet shows a much more uniform and smaller size of cavities and of dendritic pellet material than the FORM1-A partially-reacted pellet, as shown in Figure 10.8 (b). Also, the white phase in this FORM4-A pellet seems more concentrated near cavity walls than in the FORM1-A sulfided pellet.

10.5 X-ray Diffraction of Whole Pellets

One pellet from each sample was pulverized and subjected to x-ray diffraction (XRD) analysis to determine what crystalline phases were present and the degree of crystallinity of the phases. Figures 10.9 through 10.12 show for each pellet an XRD pattern trace and stick patterns of comparable standard phases found in each sample, showing location and intensity of peaks. Figures 10.9 and 10.11 show that the only crystalline phase in both fresh pellets is Mn_2AlO_4. Other phases searched for include: galaxite ($MnAl_2O_4$), (LI,Al) Mn_2O_4, hausmannite (Mn_3O_4), corundum (Al_2O_3), and bixbeyite (Mn_2O_3). Figure 10.10 shows that the major crystalline phase of the FORM4-A sulfided pellet is alabandite (MnS), as expected, that a minor crystalline phase, galaxite ($MnAl_2O_3$) is present, that Mn_2AlO_4 is absent, and that two unidentified small peaks occur at 40.6 and 66.5 degrees two-theta. Figure 10.12 shows the same for FORM1-A sulfided pellet except that only the unidentified small peak at 40.6 degree two-theta appears.

10.6 Interpretation of Results

10.6.1 Cracks

cracks create major gas channels which would help gas diffuse into the pellet, but too many might defeat diffusion of gas into smaller pores and would weaken pellets. The few cracks observed in figures presented above do not appear excessive. The figures also show very few surface cracks extending into the pellet interior, so they are apparently not a problem.

10.6.2 Cavities

Large (about 0.1 diameter of pellet) cavities in a pellet could weaken the structure and represent loss of volume of reactive material, so that they should be minimized during pellet formation and heat hardening (induration). These pellets had occasional to frequent large cavities. Both larger and smaller cavities are observed in these pellets. Smaller cavities, especially those below 100 microns (0.1 mm), would seem beneficial in conducting gas throughout a pellet. These pellets had mostly a good distribution of smaller cavities. The structure of the FORM4-A sulfided pellet shows the most desirable smaller-cavity size and distribution of the four pellets.

10.6.3 Particle Size

Particle size affects the diffusion of gas into pellet particles such that gas has to penetrate farther into larger pellet particles than smaller ones to reach the center of the particle. Also, a reaction rim (front) near the surface of a large particle may prevent further gas penetration. Larger particles in a pellet will most likely cause larger pores between particles, but the percent porosity is mostly independent of particle size and is more dependent on particle size distribution because smaller particles can fill in cavities between bridged larger particles. Permeability (interconnection of pores) is affected by particle size distribution and other factors. Pellets in this study appeared to have good porosity and permeability.

10.6.4 Phases

FORM1-A fresh pellet shows a white phase that is interpreted as Mn oxide in a gray phase that is Al_2O_3-rich and probably a non-crystalline matrix. The Mn oxide shows much interconnection within finer texture, and lesser interconnection within coarser texture. Details are much clearer at high magnification where the Mn oxide shows subhedral (partly bounded by crystal faces) grains that make contact with adjacent grains of Mn oxide. The rather coarse grain size and degree of crystal development of the Mn oxide phase is indication that the oxidation reaction to form Mn oxide went to completion. The gray phase appears less prominent because it is partly below the surface and reflects less light than at the lower magnification. Microscopy will not reveal if any Al, Ti, or Si is present in the Mn oxide phase, or if any Mn is in the gray phase. EMP element maps or point analyses are needed to determine this.

FORM4-A fresh pellet looks different from the FORM1-A fresh pellet at

low and intermediate magnification, but at higher magnification the textures of both pellets look nearly identical. The difference can be partly explained by a finer initial particle size for the FORM4-A pellet, and partly by more fusion of the Mn_2AlO_4 in the FORM1-A pellet, as if it were formed at a higher temperature or had more of a fluxing composition.

The FORM1-A sulfided pellet in Figure 10.8 shows a white phase interpreted as alabandite (MnS) and two gray phases: a lighter gray phase which appears to be the only matrix in contrast to the Mn sulfide in parts of the texture, and elsewhere appears as irregular shapes in a darker gray matrix. The gray phases are suspected to be Al_2O_3- and SiO_2-bearing, poorly- to non-crystalline material. It is noteworthy that the expected Mn sulfide phase is usually near cavity walls where it would have most access to sulfur-containing gas. It may be that the sulfidation process for this pellet did not go to equilibrium as attested by the two gray phases. Figure 10.8 shows that the rim and some distance into the pellet the texture appears fused, as though the temperature was too hot, resulting in preventing the gas from penetrating to the middle of the pellet, which looks in Figure 10.8 (b) to be unreacted from its similarity to the oxide pellet of Figure 10.7.

The FORM4-A sulfided pellet of Figure 10.6 appears to have much less fusion and more uniform penetration of sulfur-containing gas than occurred with FORM1-A sulfided pellet.

Phases in the fresh and sulfided FORM4-A pellets are similar to those observed in the two corresponding FORM1-A pellets discussed above.

10.7 X-ray Diffraction of Whole Pellets

Rather than identifying Mn_3O_4 (hausmannite) in the fresh ore- and $MnCO_3$-based pellets, the phase Mn_2AlO_4 was identified by x-ray diffraction analysis as the only crystalline phase. The original patterns, not those of figures 10.9 - 10.12, show that the peaks are only moderately sharp and the background is moderately high, an indication that: (1) the crystalline phase is not very well crystallized, and (2) there is a non-crystalline phase present that probably is the matrix. The crystalline Mn_2AlO_4 is compatible with the 1975 phase diagram for Mn_3O_4-Al_2O_3 in air, in which the cubic phase of $(Mn,Al)_3O_4$ is called spinel, and the tetragonal phase of this composition is called hausmannite. The phase produced at equilibrium in these Mn oxide pellets contains approximately two atoms of Mn and one of Al for each formula unit. It is not surprising that Al^{3+} can substitute for Mn since their ionic radii are not very different, and possibly Ti^{3+} or Ti^{4+} could substitute for Mn.

10.8 Conclusions

The important findings can be summarized as follows: cracks in the pellets do not appear to be a problem. Large cavities in the pellets during formation could cause fired pellet weakness and loss of reactive material. Aluminum is an active part of the crystalline manganese oxide phase, forming Mn_2AlO_4, or

$Mn_{2.5}Al_{0.5}O_4$. MnS is the crystalline phase of the sulfide pellets. Both aluminum and the small amount of titanium disperse throughout the pellets, and are present in both matrix and the phases Mn_2AlO_4 and MnS.

The matrix contains much Mn in both oxide and sulfide pellets and much S in the sulfide pellets. The matrix is interpreted as non-crystalline, has a rather variable composition and is believed to both support the structure and to be chemically reactive during elevated temperature reactions. The finer particle size and texture of FORM4-A pellets examined seem to favor good gas penetration and reaction, while FORM1-A pellets examined were observed to have coarser particles and texture and possibly a problem with gas penetration.

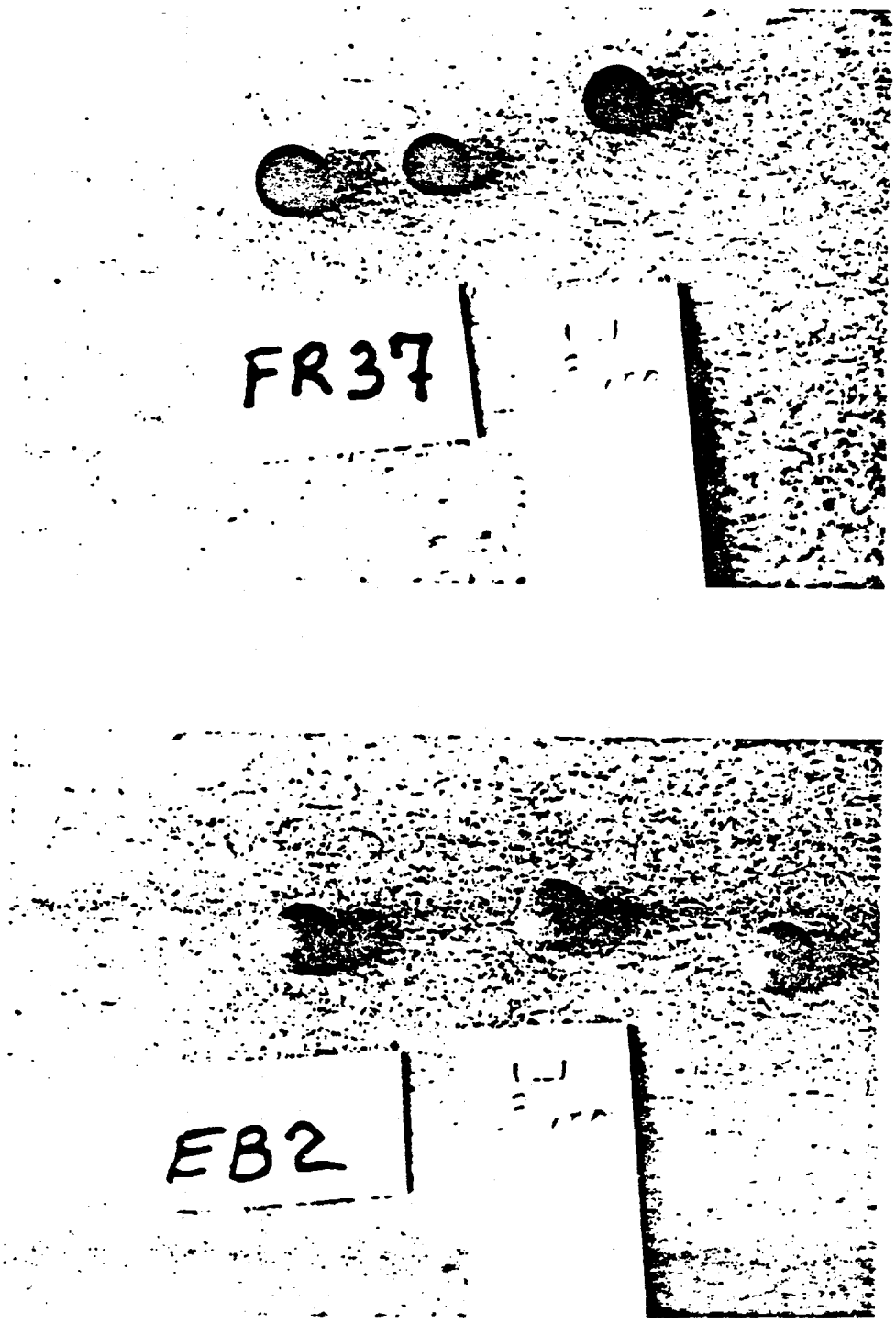

Figure 10.1 Macrophotograph of FORM4-A pellets in the (a) fresh condition and (b) partially loaded (sulfided) condition. Scale: 2.7 x actual size.

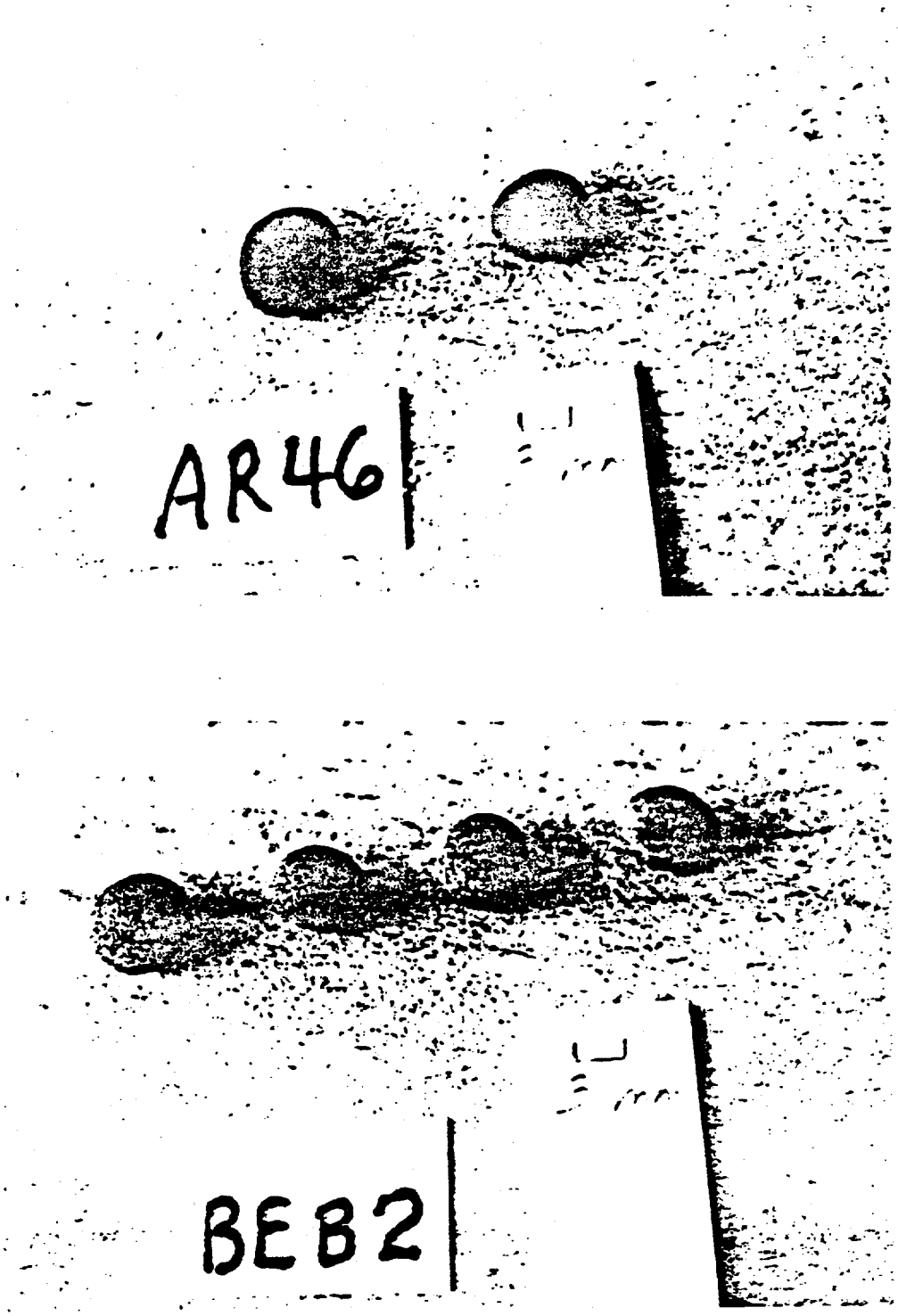

Figure 10.2 Macrophotograph of FORM1-A pellets in the (a) fresh condition and (b) partially loaded (sulfided) condition. Scale: 2.7 x actual size.

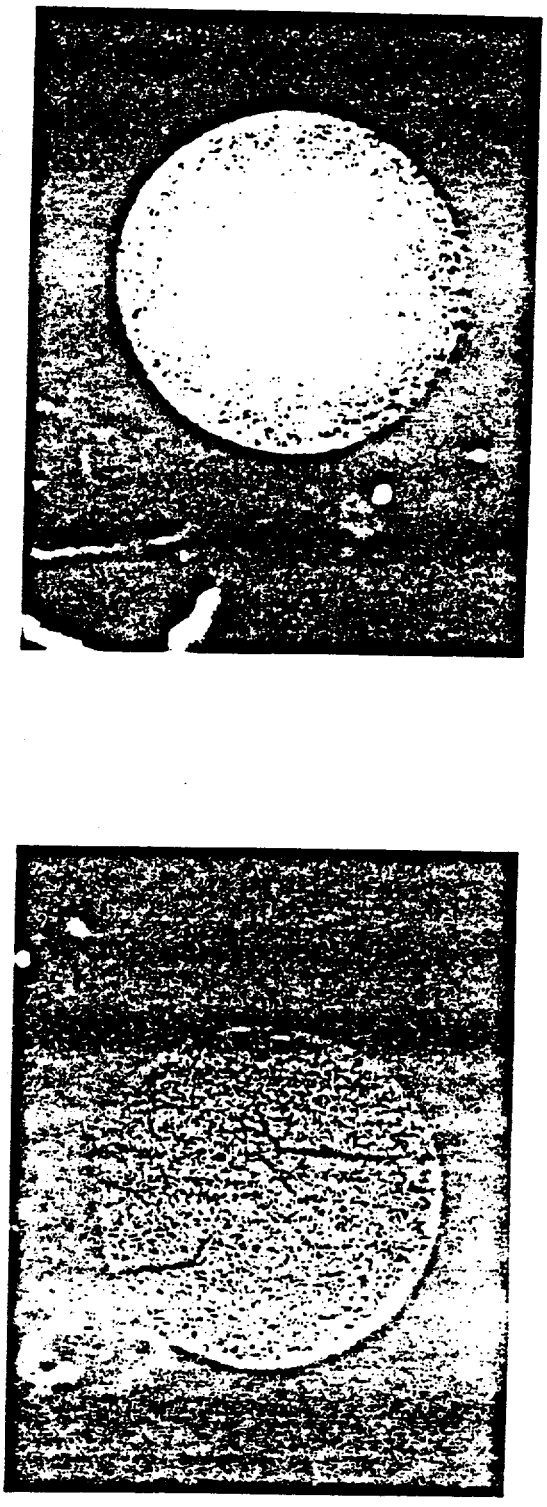

Figure 10.3 Surface texture and structure of FORM4-A pellets in the (a) fresh condition and (b) partially-loaded condition. Magnification = 12 X.

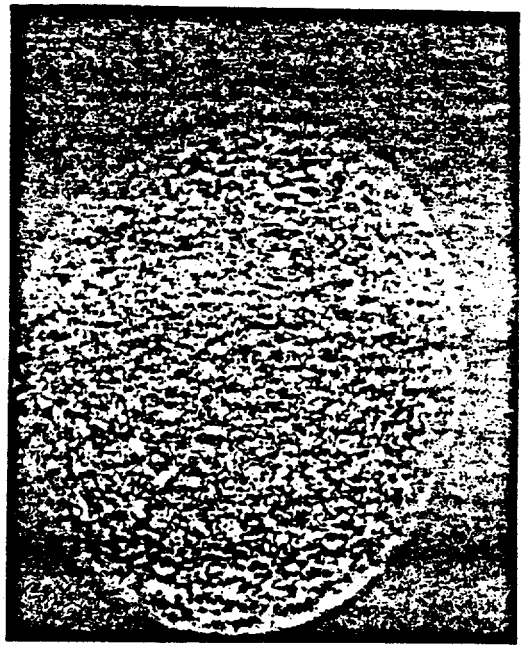

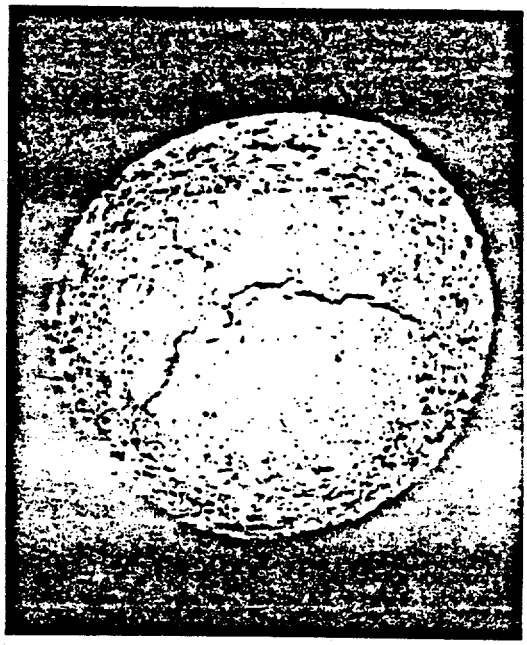

Figure 10.4 **Surface texture and structure of FORM4-1 pellets in the (a) fresh condition and (b) partially-loaded condition. Magnification= 12 X.**

Figure 10.5 Light optical photomicrograph of a FORM4-A fresh pellet, center sectioned, polished surface. Magnification= 34 X (a) and (b) an enlargement of area shown on (a). Magnification= 118 X. [white= Mn oxide; gray= matrix; black= cavities]

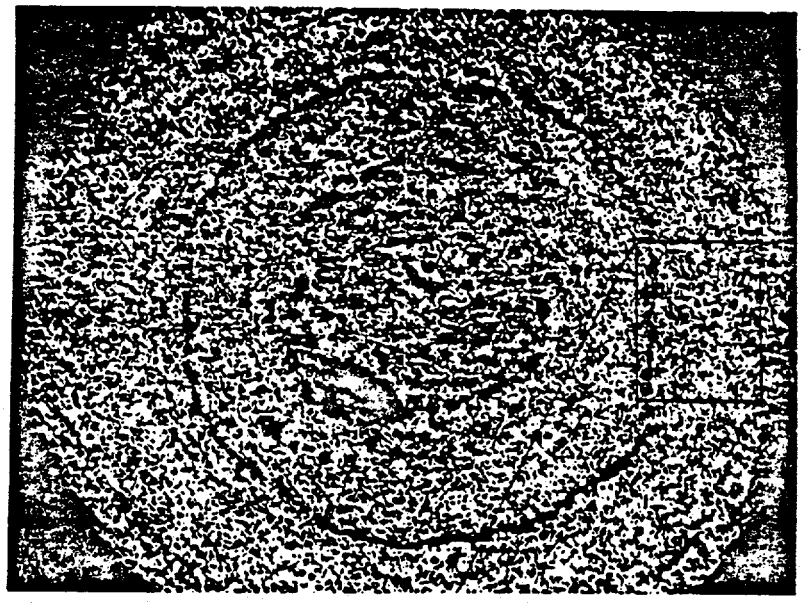

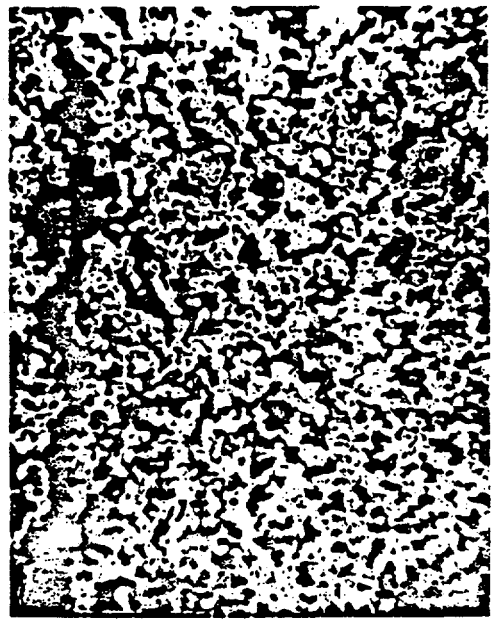

Figure 10.6 Light optical photomicrograph of a FORM4-A partially-sulfided pellet, center sectioned, polished surface. Magnification= 34 X (a) and (b) an enlargement of area shown on (a). Magnification= 118 X. [white= Mn sulfide; gray= matrix; black= cavities]

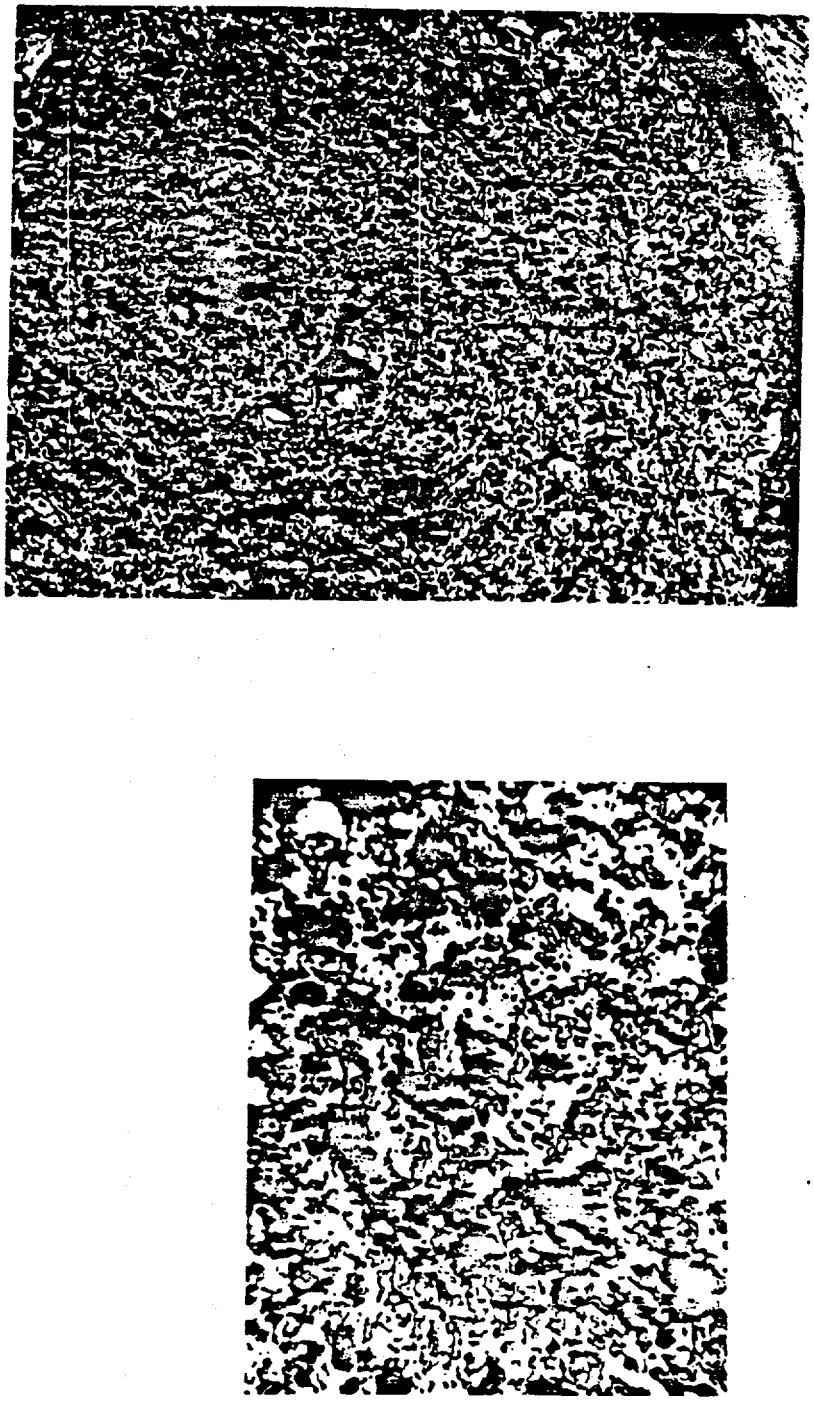

Figure 10.7 Light optical photomicrograph of a FORM1-A fresh pellet, center sectioned, polished surface. Magnification= 34 X (a) and (b) an enlargement of area shown on (a). Magnification= 118 X. [white= Mn oxide; gray= matrix; black= cavities]

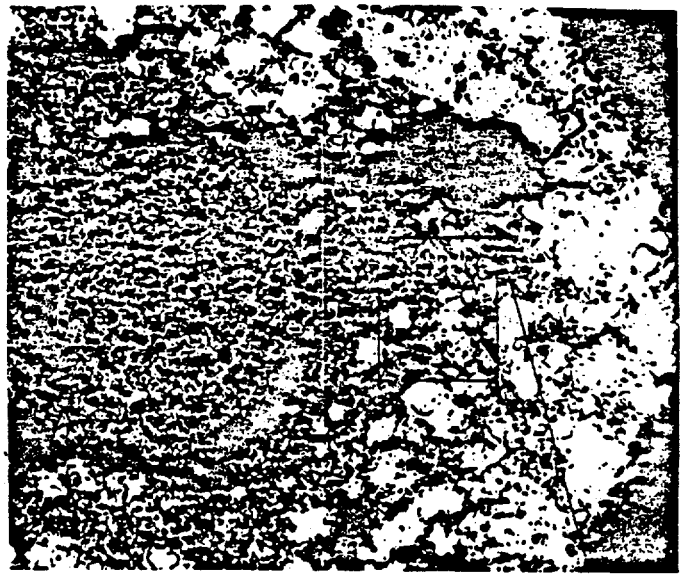

Figure 10.8 Light optical photomicrograph of a FORM1-A partially-sulfided pellet, center sectioned, polished surface. Magnification= 34 X (a) and (b) an enlargement of area shown on (a). Magnification= 118 X. [white= Mn sulfide; gray= matrix; black= cavities]

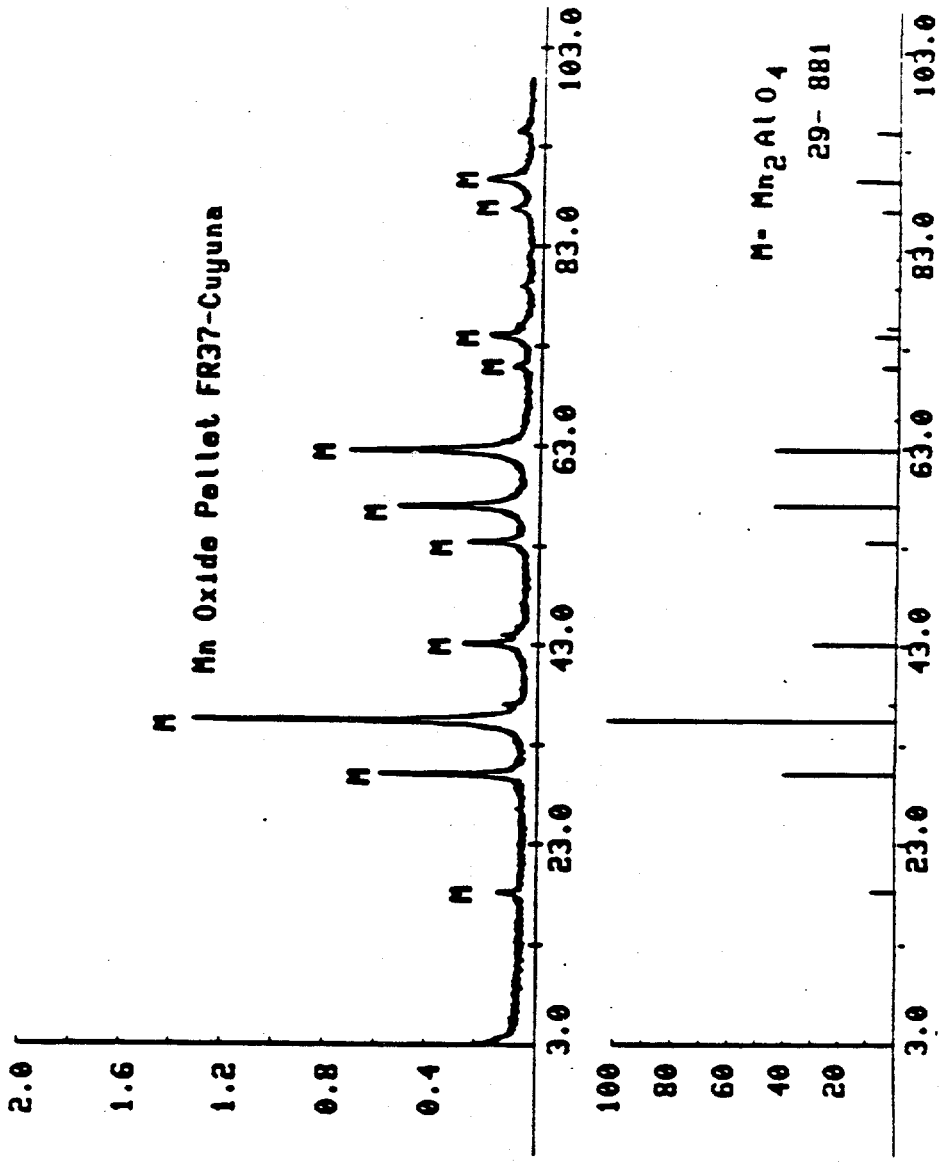

Figure 10.9 Fresh FORM4-A whole pellet XRD pattern. The only crystalline phase present is Mn_2AlO_4.

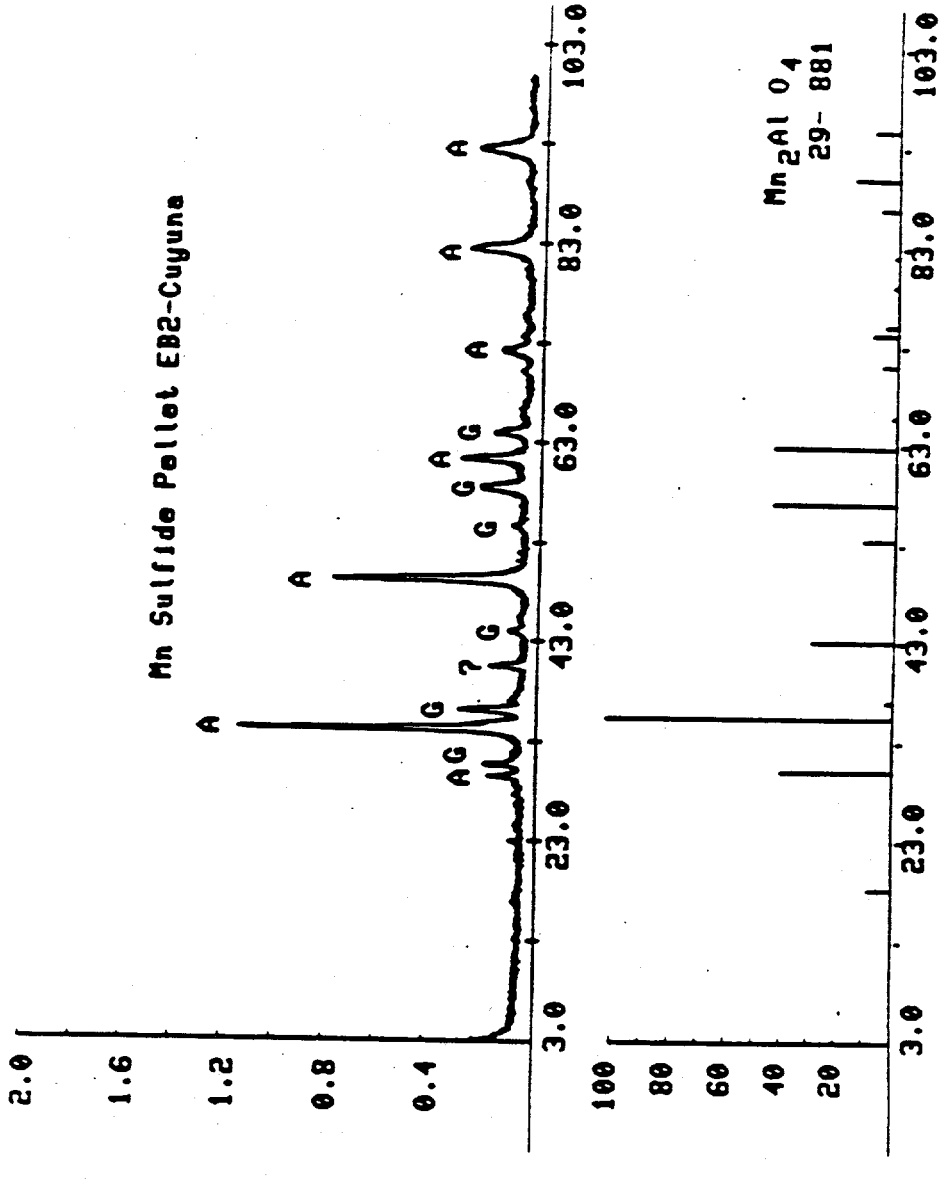

Figure 10.10 XRD pattern of partially-reacted FORM4-A pellet. Major phase is alabandite (MnS).

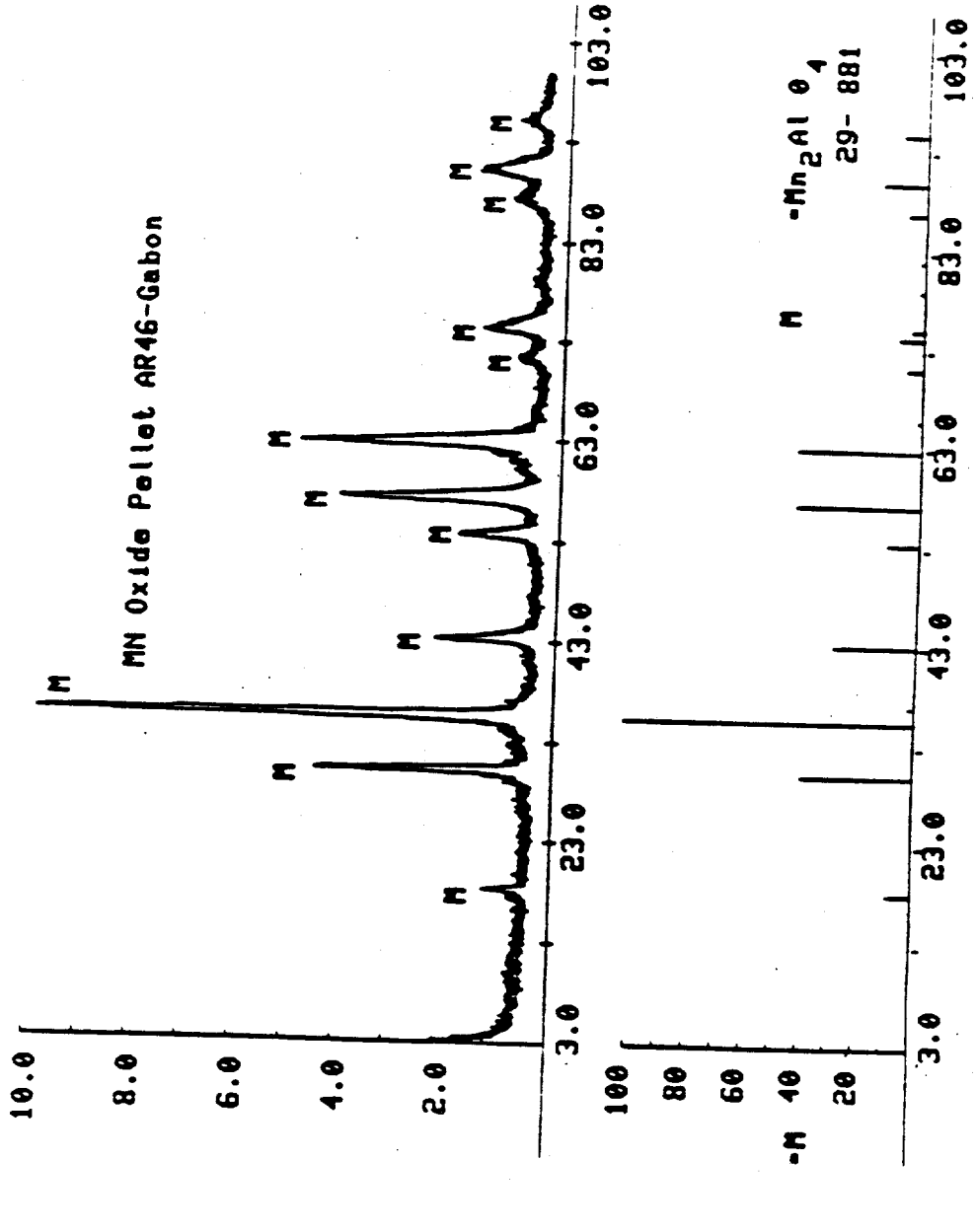

Figure 10.11 Fresh FORM1-A whole pellet XRD pattern. The only crystalline phase present is Mn_2AlO_4.

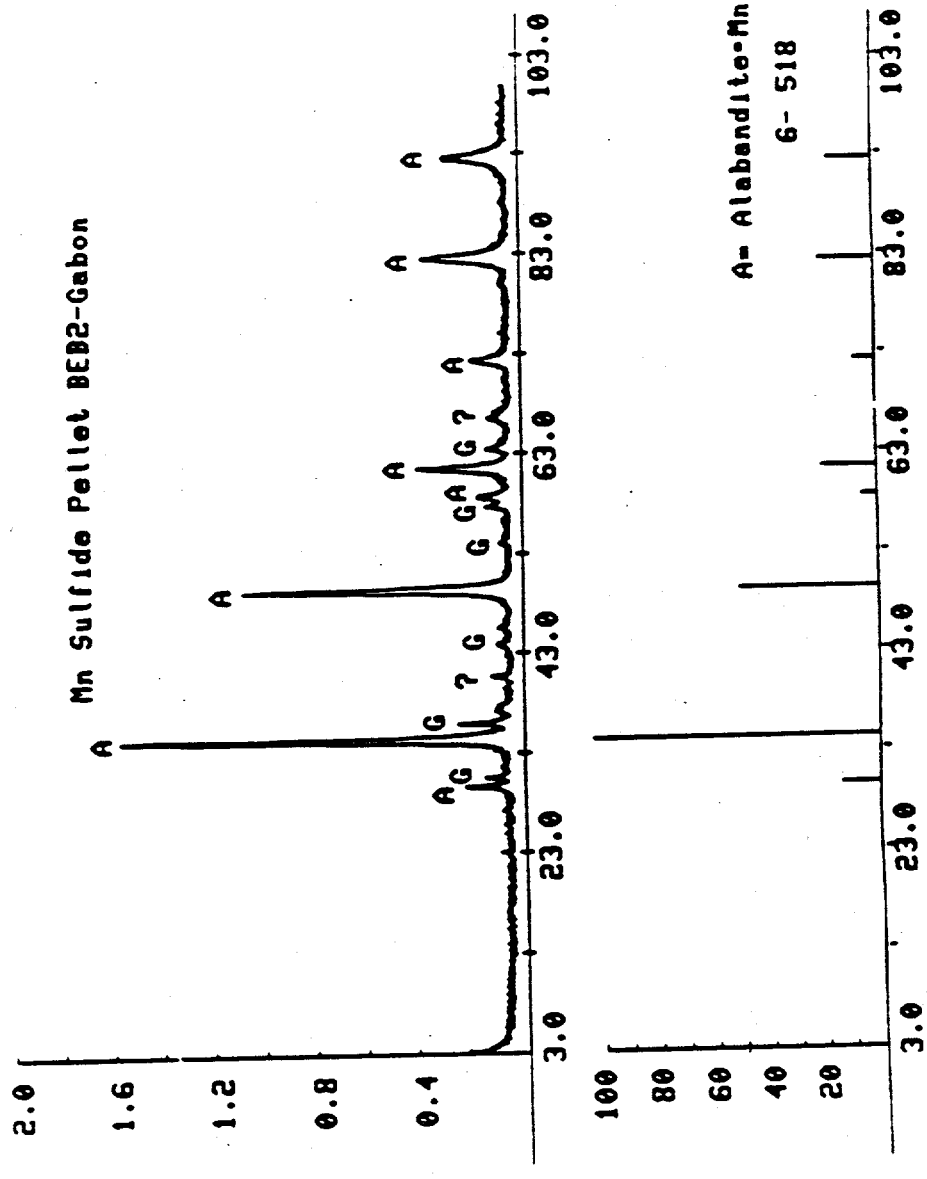

Figure 10.12 XRD pattern of partially-reacted FORM1-A pellet. Major phase is alabandite (MnS).